Title	Development of fuel performance analysis code, BISON for MOX, named Okami; Analyses of pore migration behavior to affect the MA-bearing MOX fuel restructuring
Author(s)	Ozawa Takayuki, Hiroka Shun, Kato Masato, Novascone S., Medvedev P.
Citation	Journal of Nuclear Materials,553,p.153038_1-153038_16
Text Version	Accepted Manuscript
URL	https://jopss.jaea.go.jp/search/servlet/search?5070644
DOI	https://doi.org/10.1016/j.jnucmat.2021.153038
Right	© 2021. This manuscript version is made available under the CC-BY-NC-ND 4.0 license http://creativecommons.org/licenses/by-nc-nd/4.0/. This is the accepted manuscript version. The formal published version is available at https://doi.org/10.1016/j.jnucmat.2021.153038 .

Title:

Development of fuel performance analysis code, BISON for MOX, named Okami: Analyses of pore migration behavior to affect the MA-bearing MOX fuel restructuring

Authors & affiliations:

Takayuki Ozawa[a], Shun Hirooka[a], Masato Kato[a],

Stephen Novascone[b], Pavel Medvedev[b]

Corresponding author: ozawa.takayuki@jaea.go.jp (T. Ozawa)

[a] Japan Atomic Energy Agency, 4002 Narita-cho, Oarai-machi, Ibaraki 311-1393, Japan

[b] Idaho National Laboratory, 1955 N. Fremont Ave., Idaho Falls, ID 83415, USA

HIGHLIGHTS:

- 2-D analyses with modelling for MOX fuel restructuring in use of fast reactor.
- Effects of O/M ratio and pellet-cladding gap width on pore migration behavior.
- Irradiation behavior evaluation for the MA-bearing MOX irradiation test in Joyo.
- Influence of pellet eccentricity on central void formation in 2-D analyses.

Abstract:

Fuel composition, i.e. Pu content, minor actinide (MA) content, oxygen-to-metal (O/M) ratio, etc., affects the irradiation behavior of MA-bearing mixed oxide (MOX) for fast reactor. To evaluate the O/M dependence of pore migration regarding fuel restructuring at the beginning of irradiation, we are developing BISON for MOX in cooperation with Idaho National Laboratory (INL) and have installed a pore migration model considering

vapor pressure of vapor species and thermal conductivity for MOX. The O/M dependence of fuel restructuring observed in MA-bearing MOX irradiation in the experimental fast reactor Joyo was evaluated by a two-dimensional (2-D) analysis. To solve partial differential equations for energy conservation and advection diffusion equations to calculate temperature and pore migration, respectively, a correlation of thermal conductivity as a function of porosity, temperature, deviation from stoichiometry, Am content and Np content was used. In addition, the pore migration velocity was calculated by using a correlation depending on vapor pressure applying Rand-Markin's model.

Four MA-bearing MOX test pins with different O/M ratio and pellet/cladding gap size were irradiated in B14 test in Joyo to study the effects of O/M ratio and gap size on irradiation behavior at the beginning of irradiation. In post-irradiation examinations (PIE), a remarkable restructuring was observed in stoichiometric fuels, and a discrepancy in central void diameter among various O/M ratios. This restructuring behavior could be evaluated by considering the influence of O/M ratio on vapor pressure. Also, a central void is assumed to offset from the geometric center to the larger-gap side due to the pellet eccentricity, but the PIE results were inconsistent in this regard. It is expected that the irradiated pellet might displace to another side during sample preparation in PIE from a reverse offset location during irradiation by comparing the result of 2-D analysis and radial profile of fuel density.

Keywords; MA-bearing MOX fuel for fast reactor, Pore migration behavior, Irradiation experiments in Joyo, 2-D analyses, BISON

1. Introduction

Japan Atomic Energy Agency (JAEA) and Idaho National Laboratory (INL) are developing a multi-dimensional fuel performance analysis code for fast reactor mixed-oxide (MOX) fuel. This international collaboration is established through the Civil Nuclear Energy Working Group (CNWG) between Japan and the US. JAEA has leveraged its experience with MOX properties and models to extend the fuel performance capabilities of BISON [1], an engineering-scale fuel performance application developed at INL. Thermal and restructuring behavior of MOX fuel in fast reactors is now represented in BISON with the addition of MOX fuel properties and models for thermal conductivity [2], oxygen potential [3], and vapor pressure [4]. These additional features have been complied to form a new BISON application named “Okami”, which means a wolf in Japanese.

Fuel restructuring caused by pore migration, which is due to a steep radial temperature gradient, is one of the most remarkable behaviors of MOX fuels irradiated in fast reactors. A first modeling of this mechanism was previously installed in BISON [5], by introducing finite element computations in the resolution of advection diffusion. This prior work has been completed in Okami by accounting for the effects of fuel composition on the mechanism. In order to study fuel behaviors in the early stage of irradiation, a short-term irradiation test with Am-bearing MOX fuels, referred to as the B14 test, was conducted in Joyo; a sodium-cooled fast reactor located in O-arai, Ibaraki, Japan. In the B14 test, the influence of diametric gap size and oxygen-to-metal (O/M) ratio on the thermal behavior of the fuel pellet were recorded during observation of post-irradiation examinations (PIE).

Okami is capable of simulating pore migration and the corresponding fuel

restructuring at early stages of irradiation. The effects of the diametric gap size and O/M ratio, observed in PIE for MOX fuels irradiated in B14, and the influence of pellet eccentricity were compared to 2-D Okami calculations. This comparison and corresponding discussion are presented in this study, which demonstrates Okami's ability to accurately represent the complex behavior of fuel restructuring in a sodium-cooled fast reactor.

2. Code development

The fuel performance analysis code, CEPTAR [6], has been developed at JAEA for design and analysis of annular oxide fuel irradiated in fast reactors. CEPTAR has been verified by using the irradiation tests in EBR-II in the US, Phenix in France, PFR in the UK, and Joyo in Japan [6]. In order to develop a multi-dimensional fuel performance code for fast reactor MOX fuels, the analysis models for oxide fuel in CEPTAR were installed in BISON under the international collaboration of the CNWG.

2.1 Thermal analysis model

Fuel temperature is calculated by solving the following general partial differential equation:

$$\rho C \cdot \partial T/\partial t - \nabla \cdot \lambda \nabla T - q = 0 \quad (1)$$

where ρ is density, C is specific heat, T is temperature, t is time, λ is thermal conductivity and q is the heat source. The following thermal conductivity, which is applicable to MOX and minor-actinide (MA)-bearing MOX fuels [2] was applied.

$$\lambda = \frac{1-p}{1+p/2} \cdot \left(\frac{1}{g(x, Am, Np, T)} + \frac{A}{T^{2.5}} exp\left(-\frac{B}{T}\right) \right) \quad (2)$$

where p is porosity; a unitless fraction of void space to fully dense fuel volume, A and B are constants ($A = 1.541 \times 10^{11}$, $B = 1.522 \times 10^{4}$). The function, g, is defined as

follows:

$$g(x, Am, Np, T) = (2.713x + 3.583 \times 10^{-1} z_1 + 6.317 \times 10^{-2} z_2) + (-2.625x + 2.493) \times 10^{-4} T \quad (3)$$

where x is the stoichiometric deviation in $MO_{2.00-x}$, z_1 is Am content and z_2 is Np content. Comparing the thermal conductivity between MOX and 5 wt.% Am-bearing MOX with Pu content of 30 wt.% and porosity of 0.10, the dependence of O/M ratio on thermal conductivity is shown in Fig. 1. The dependence of Am content on thermal conductivity at 2,273 K for O/M ratios of 1.96, 1.98 and 2.00 with Pu content of 30 wt.% and porosity of 0.10 is shown in Fig. 2. These figures show that the fuel is most thermally conductive at stoichiometric conditions and that fuel thermal conductivity decreases as O/M ratio decreases and as Am content increases.

The effect of burnup on fuel thermal conductivity is greatly important and a necessary feature to include when validating a fuel performance code. However, the effect of burnup has not been applied to the MOX thermal conductivity model in Okami. The effect of burnup has to be developed and applied in the next phase of code development. For the present study, neglecting the effect of burnup on fuel thermal conductivity remains a justified assumption, since the B14 tests to be considered are short-term irradiations.

2.2 Pore migration model

Fuel restructuring caused by pore migration in the presence of a steep radial temperature gradient is one of remarkable behaviors of MOX fuels irradiated in fast reactors. As shown in Ref. [5], pore migration can be simulated by solving the following partial differential equation of advection diffusion with porosity (p) as the primary variable:

$$\partial p/\partial t + \nabla \cdot [(1-p)p\vec{v} - \upsilon \cdot \nabla p] = 0 \quad (4)$$

where $\vec{v}$ is pore migration velocity and υ is an effective diffusion coefficient. A value of p=1 represents a central void and p=0 represents maximum mass density. The term $(1-p)p\vec{v}$ is used to ensure that porosity is always between 0 and 1 and that the pore velocity term is active only for values of porosity between 0 and 1 because pore movement is non-existent in regions full of pores (p=1) and in regions without pores (p=0). It is well known that pore migration is caused by the evaporation-condensation mechanism in a pore, and the corresponding pore migration velocity $\vec{v}$ is calculated from the following equation [6,7].

$$\vec{v} = \Omega \cdot D \cdot \, d/dT \, (P/kT) \cdot \nabla T \tag{5}$$

where Ω is molecular volume [8], D is diffusion coefficient, P is vapor pressure and k is Boltzmann's constant. The vapor pressure P can be calculated from a correlation between vapor pressure of vapor species and Gibbs free energy by applying Rand-Markin's model [4,9].

$$m = x/q \tag{6}$$

$$n = x/r \tag{7}$$

$$p(\mathrm{UO_2}) = (1-q-r)\, exp\left(-\frac{\Delta G^{\circ}_{\mathrm{UO_2,vap}}}{RT}\right) \tag{8}$$

$$p(\mathrm{PuO_2}) = qp(O_2)^{\frac{m}{2}}\, exp\left(-\frac{\Delta G^{\circ}_{A}}{RT}\right) \tag{9}$$

$$\Delta G^{\circ}_{A} = -\frac{1}{2}\int_0^m RT\, ln\, p\,(O_2)\, dm' + \Delta G^{\circ}_{\mathrm{PuO_2,vap}} \tag{10}$$

$$p(\mathrm{UO}) = \frac{p(\mathrm{UO_2})}{exp\left(-\frac{\Delta G^{\circ}_{\mathrm{UO/UO_2}}}{RT}\right)p(O_2)^{1/2}} \tag{11}$$

$$p(U) = \frac{p(\mathrm{UO})}{exp\left(-\frac{\Delta G^{\circ}_{\mathrm{U/UO}}}{RT}\right)p(O_2)^{1/2}} \tag{12}$$

$$p(\mathrm{UO_3}) = exp\left(-\frac{\Delta G^{\circ}_{\mathrm{UO_2/UO_3}}}{RT}\right)p(\mathrm{UO_2})p(O_2)^{1/2} \tag{13}$$

$$p(\mathrm{PuO}) = \frac{p(\mathrm{PuO_2})}{exp\left(-\frac{\Delta G^{\circ}_{\mathrm{PuO/PuO_2}}}{RT}\right) p(O_2)^{1/2}} \quad (14)$$

$$p(\mathrm{Pu}) = \frac{p(\mathrm{PuO})}{exp\left(-\frac{\Delta G^{\circ}_{\mathrm{Pu/PuO}}}{RT}\right) p(O_2)^{1/2}} \quad (15)$$

$$p(\mathrm{AmO_2}) = rp(O_2)^{n/2}\, exp\left(-\frac{\Delta G^{\circ}_{B}}{RT}\right) \quad (16)$$

$$\Delta G^{\circ}_{B} = -\frac{1}{2}\int_0^n RT\, ln\, p\,(O_2)\, d'n + \Delta G^{\circ}_{\mathrm{AmO_2,vap}} \quad (17)$$

$$p(\mathrm{AmO}) = \frac{p(\mathrm{AmO_2})}{exp\left(-\frac{\Delta G^{\circ}_{\mathrm{AmO/AmO_2}}}{RT}\right) p(O_2)^{\frac{1}{2}}} \quad (18)$$

$$p(\mathrm{Am}) = \frac{p(\mathrm{AmO})}{exp\left(-\frac{\Delta G^{\circ}_{\mathrm{Am/AmO}}}{RT}\right) p(O_2)^{1/2}} \quad (19)$$

where $p(\mathrm{i})$ are the vapor pressures of the different species normalized with normal pressure (1 atm), x is stoichiometric deviation in $\mathrm{MO_{2.00-x}}$, q is Pu fractional content, r is Am fractional content, $\Delta G^{\circ}_{\mathrm{i}}$ are the Gibbs free energies, R is the gas constant and T is temperature in Kelvin (K). The Gibbs free energies $\Delta G^{\circ}_{\mathrm{i}}$ are calculated as:

$$\Delta G^{0}_{UO_2,vap} = 567000 - 150 \cdot T \quad (20)$$

$$\Delta G^{0}_{PuO_2,vap} = 571000 - 150 \cdot T \quad (21)$$

$$\Delta G^{0}_{UO/UO_2} = -471000 + 71 \cdot T \quad (22)$$

$$\Delta G^{0}_{U/UO} = -528000 + 62 \cdot T \quad (23)$$

$$\Delta G^{0}_{UO_2/UO_3} = -404000 + 90 \cdot T \quad (24)$$

$$\Delta G^{0}_{PuO/PuO_2} = -352000 + 69 \cdot T \quad (25)$$

$$\Delta G^{0}_{Pu/PuO} = -498000 + 46 \cdot T \quad (26)$$

$$\Delta G^{0}_{AmO_2,vap} = -RT \cdot ln10^{\left(7.28-\frac{28260}{T}\right)} \quad (27)$$

$$\Delta G^{0}_{AmO/Am} = (-137700 - 28.8 \cdot T) - (263650 - 112.32 \cdot T) \quad (28)$$

$$\Delta G^{0}_{AmO_2/Am} = (-388300 + 30.7 \cdot T) - (263650 - 112.32 \cdot T) \quad (29)$$

Also, the normalized oxygen partial pressure $p(O_2)$ expressing a dependence on Pu and MA concentration and O/M ratio, based on the point defect model, of which the detailed calculation method is given in Ref. [3], was applied to calculate the vapor pressure P. Once the $p(O_2)$ are determined from Pu and MA concentration and O/M ratio, each vapor pressure of each vapor species can be calculated from Eqs. (6)-(29) and the total vapor pressure, P, is given as the sum of all the individual vapor pressures.

Comparing the oxygen potential, described by $dGO_2=RTln(O_2)$, between MOX and 5 wt.% Am-bearing MOX with Pu content of 30 wt.%, the dependence of the O/M ratio on oxygen potential at 1,273-2,073 K and total vapor pressure at 1,800-2,600 K is shown in Fig. 3 and Fig. 4, respectively. It can be seen that the oxygen potential and the vapor pressure increase with increasing O/M ratio, Am content, and temperature. In addition, Fig. 5 shows the O/M ratio dependence of the vapor pressure of each vapor specie at 2,273 K and of the total vapor pressure, for 5 wt.% Am-bearing MOX with Pu content of 30 wt.%. It can be seen that the total vapor pressure increases remarkably at O/M=2.00 and that the vapor pressure of UO_3 is dominant to decide total vapor pressure.

The effects of O/M ratio and Am content on pore migration velocity were evaluated by using the thermal analysis model and the pore migration model including vapor pressure and oxygen potential mentioned above. Fig. 6 shows the effect of O/M ratio on fuel temperature and pore migration velocity at a linear power of 36 kW/m. In these calculations, the O/M ratio was assumed to be constant along the radius of the fuel. Future development will include the effect of radially varying O/M ratios. As indicated in Fig. 6, fuel temperature decreases as O/M ratio increases due to higher thermal conductivity at larger O/M ratios (see Fig. 1). Fig. 6 also indicates the pore migration velocity increases

rapidly as the O/M ratio increases, especially in stoichiometric MOX. This is an interesting observation when considering the relatively low temperature gradient in stoichiometric fuel. To quantify the effect of O/M ratio the values of temperature, total vapor pressure, and pore migration velocity were calculated for the case of the O/M ratio ranging from 1.96 to 2.00. All of these results were divided by their respective values at an O/M ratio of 1.96. After this calculation the values for temperature, total vapor pressure, and pore migration velocity are equal to 1 when the O/M ratio is 1.96. As the O/M ratio is increased to 2.00 the values for temperature, total vapor pressure, and pore migration velocity will deviate from 1, thus normalizing for the purposes of comparison the changes in these values due to changes in O/M ratio. Fig. 7 shows the results of this comparison process for the case of Am content of 5 wt.% at a location within the fuel of r/R = 0.2, where pore migration velocity was the maximum. Fig. 7 indicates that temperature slightly decreases as the O/M ratio increases. Total vapor pressure also decreased with increasing O/M ratio up to O/M = 1.99, yet as O/M increased from 1.99 to 2.00 the total vapor pressure rapidly increased, approximately by a factor of 5 compared to the value at O/M = 1.96. This could be explained by the increase of vapor pressure of UO_3, which was a major vapor species in oxide fuels [9]. The O/M dependence of pore migration velocity followed that of total vapor pressure.

Fig. 8 shows the effect of Am content on fuel temperature and pore migration velocity at a linear power of 36 kW/m. It can be seen that the fuel temperature would increase in higher Am content due to the corresponding lower thermal conductivity (see Fig. 2). A normalized comparison calculation, similar to that previously described for Fig. 7, for factors of temperature, total vapor pressure and pore migration velocity is shown in Fig 9, where Am content is varied from 0 to 5 wt.%; again at r/R = 0.2 where pore migration

velocity was maximum. Even though (as shown in Fig. 1) thermal conductivity of Am-bearing MOX was lower than that of MOX without Am content, the temperature only slightly increases as Am content increases from 0 to 5 wt.%. On the other hand, total vapor pressure and pore migration velocity linearly increased by a factor between 2.5 and 3 with the increase of Am content from 0 to 5 wt.%.

2.3 Model verification through benchmark exercises

For the purpose of verifying model installation in Okami, benchmark exercises of fuel temperature and porosity calculations using Eqs. (1) - (5) were conducted to compare the calculation results of Okami and CEPTAR; the latter being verified for MOX fuel performance calculations in fast reactors [6]. Model conditions of the benchmark exercises are shown in Table 1. The pore migration flux at outer surface was assumed to be zero in both exercises. In Okami, formation of the central void has no impact on the finite element mesh geometry, rather the value of porosity is calculated at every point in the original domain. Heat generation was assumed to depend on the porosity; namely, the heat generation was assumed to be zero where the porosity was 1.0 corresponding to a central void area. CEPTAR, in contrast to Okami, does update the calculation domain as the central void is formed. This is an important difference to keep in mind when comparing calculation results from the two codes.

Verification consisted of two benchmark exercises: 1. Code-to-code comparison between CEPTAR and Okami in which porosity and temperature calculations are compared along the radius of the fuel and 2. Okami calculations to assess the effects of O/M ratio and Am content on fuel temperature and porosity.

2.3.1 Code-to-code comparison between CEPTAR and Okami for thermal analysis and pore migration in MOX fuel

In the first benchmark exercise, the fuel is represented with a one-dimensional (1-D) axisymmetric mesh in both codes with dimensions of 4.1 mm radius and 100 mm height (note height is specified for the purpose of defining volumetric power). The initial condition for porosity and temperature was 0.12 and 1,400 K respectively. In addition, the boundary conditions were defined for the outer surface temperature to be 1,400 K and the pore migration flux at boundary (outer surface) was assumed to be zero. The power history assumed in this exercise is shown in Fig. 10. The power increased to 38 kW/m from initial conditions in 80,000 s at the rate of 4.5 %/h and then held for 70,000 s.

Calculation results for MOX with Pu content of 20 wt.% and O/M ratio of 1.98 are shown in Fig. 11 and Fig. 12. Fig.11 shows a comparison of fuel temperature and porosity, and Fig. 12 shows a comparison of fuel temperature and pore migration velocity between CEPTAR and Okami at an elapsed time of 150,000 seconds. Also, Fig. 13 and Fig. 14 show corresponding results for stoichiometric O/M. As porosity increases in the center of the fuel, recall that CEPTAR's calculation domain (mesh geometry) changes to accommodate central void formation where Okami's domain is constant. Therefore, the calculation results in Figs. 11-14 show Okami results along the entire fuel radius and CEPTAR results in a region between the inner surface of the central void and the outer surface of the fuel. Observation of Fig. 11-14 indicate fuel temperature, porosity, and pore migration velocity calculated with Okami is similar to that of CEPTAR, thus verifying proper implementation of models and properties from CEPTAR to Okami.

2.3.2 Assessment of Okami calculations regarding the effects of O/M ratio and Am content on fuel temperature and porosity

Using the favorable comparison between CEPTAR and Okami as a basis, the effects of O/M ratio and Am content were evaluated in a second benchmark exercise. This

benchmark consisted of a 1-D axisymmetric calculation domain with 2.675 mm radius and 100 mm height. The initial fuel density was assumed to be 0.85 (porosity was 0.15). In this problem, the power increased to 45 kW/m in 10,000 s, and then held for 5,000 s. The initial temperature was assumed as 630 K, and the outer surface temperature was assumed to increase from the initial temperature of 630 K to 1,000 K during the initial power increase in 10,000 s, and then held at 1,000 K for 5,000 s as a boundary condition. Plots of power history and the outer surface temperature are shown in Fig. 15.

A comparison of maximum fuel temperature and radial peak porosity near the pellet center for MOX with Pu content of 20 wt.% and varying O/M ratios of 1.96, 1.98 and 2.00, calculated with Okami, is shown in Fig. 16. Due to the O/M influence on fuel thermal conductivity, the fuel temperature at an O/M ratio of 1.96 was the highest where an O/M ratio of 2.00 resulted in the lowest temperature. It's important to note that the predicted temperatures were simply consistent with the adopted boundary condition and are likely higher than those encountered in a real fuel pin due to the exclusion of important physics such as fuel-to-clad gap closure and the corresponding increase in thermal conductance. According to these calculations, the porosity in fuel with an O/M ratio of 1.96 reached its maximum of 1.0 faster than fuel with higher O/M ratios, where fuel with an O/M ratio of 2.00 took the most time in reaching maximum porosity. In addition, Fig. 17 shows a comparison of radial fuel temperature and porosity, calculated at elapsed time of 150,000 s, with O/M ratios of 1.96, 1.98 and 2.00. In Fig. 16 the central void region is defined where porosity is 1.0. Using this definition, Fig. 16 indicates that the largest central void is found in stoichiometric fuel even though stoichiometric fuel temperature was the lowest. This was consistent with a tendency for vapor pressure to be the highest in O/M ratio of 2.00 (See Fig. 4). In summary, the calculation results with Okami indicate

that fuel temperature was the lowest, pore migration was the slowest, and perhaps counterintuitively, the amount of radially migrating pores (central void formation) was highest in stoichiometric MOX. These trends will be validated through a comparison against experimental data in section 4.1.

The sensitivities of Am content on fuel temperature and pore migration were also studied for this benchmark exercise. A comparison of maximum fuel temperature and radial peak porosity near the pellet center between MOX and 5 wt.% Am-MOX, calculated with Okami, are shown in Fig. 18. Pu content and O/M ratio for MOX and 5 wt.% Am-MOX was fixed to be 20 wt.% and 1.98, respectively. Due to the reduction of fuel thermal conductivity caused by Am content, the fuel temperature in 5 wt.% Am-MOX was higher than that in MOX during the initial power increase (0 - 10,000 s), and the maximum fuel temperature in both fuels were almost the same after the central void formation. Also, the radial peak porosity in 5 wt.% Am-MOX began to increase and reached 1.0 earlier than that in MOX with the increase of fuel temperature. In addition, Fig. 19 shows a comparison of radial fuel temperature and porosity between MOX and 5 wt.% Am-MOX, calculated at an elapsed time of 150,000 s. Again, due to the reduction of fuel thermal conductivity caused by Am content, the fuel temperature in 5 wt.% Am-MOX was higher than that in MOX, which seems to be the reason for the larger central void found in 5 wt.% Am-MOX than that in MOX. Thus, it was confirmed that Okami correctly calculates the effect of O/M ratio and Am content on pore migration behavior by taking into account their influence on fuel properties such as thermal conductivity and vapor pressure.

3. Irradiation experiment

In order to study fuel behaviors in the early stage of irradiation, a short-term irradiation test with MA-bearing MOX fuels, specifically the B14 test, was conducted in Joyo. The major specifications of four test pins; PTM001, PTM002, PTM003 and PTM010, irradiated in B14 are shown in Table 2. As-fabricated Pu content and Am content was specified to be 31 wt.% heavy metal (HM) and 2.4 wt.% HM, respectively. In the B14 test, the diametric gap size and O/M ratio were defined as test parameters to evaluate the influence of these parameters on fuel restructuring. PTM001 was a reference pin, PTM002 had a large diametric gap size (210 μm), PTM003 had lower O/M ratio (1.96), and PTM010 had both larger diametric gap and stoichiometric O/M. These four test pins were irradiated with two dummy pins in each compartment loaded to the un-instrumented fuel subassembly B, UNIS-B, as shown in Fig. 20.

The history of reactor power and corresponding local peak linear power during the B14 test is shown in Fig. 21. After the normal starting operation, the reactor power was held at 92% (35 kW/m) of nominal power for 24 hours in the first power step, 102% (39 kW/m) for 24 hours in the second power step, and then, increased to 125% (47 kW/m) as a transient level and held for 10 minutes followed by a rapid shutdown. The power increase rate among each power level was 0.4 %/min.

The influence of O/M ratio on central void diameter obtained in the PIE is shown in Fig. 22. Central void diameter measured with ceramography and X-ray CT are plotted in this figure. The central void in PTM003 with an O/M ratio of 1.96 tended to be larger than that in PTM001 with O/M ratio of 1.98. This is expected to be caused by lower fuel temperature in PTM001 due to the O/M influence on fuel thermal conductivity. Also, for the case of fuel with an O/M ratio of 1.98, there was another test pin with larger gap size, PTM002. The larger gap size, and corresponding lower thermal gap conductance, of

PTM002 resulted in a larger central void than that found in PTM001. On the other hand, the central voids in stoichiometric PTM010 tended to be larger than those in any other B14 test pin though fuel temperature in PTM010 is lower than that in other test pins with lower O/M ratio. This acceleration of pore migration in stoichiometric MOX is expected to be caused by enhanced vapor pressure at O/M ratio of 2.00 as mentioned above and shown in Fig. 6 and Fig. 7.

4. Analysis and discussion on the pore migration behavior

4.1 Effect of O/M ratio

The effects of O/M ratio on pore migration behavior could be observed in PIE for B14 test pins. Using Okami, the radial profiles of fuel temperature and porosity were calculated for ceramographs at axial core center in 2-D cartesian analyses. The 2-D calculation results of pore migration for PTM001 with a reference O/M (1.982) and a diametric gap size (160 μm) and PTM010 with a stoichiometric O/M (1.999) and a larger diametric gap size (210 μm) during the B14 test is shown in Fig. 23 and Fig. 24, respectively. As shown in these figures, pores began to migrate radially in both test pins during the first power step for 24 hours, and then continued to migrate after the power level up to the second power step. A central void is expected to appear during the second power step and to form clearly at the final power corresponding to the transient conditions. It can be seen that the central void formation in PTM010 would be more accelerated than that in PTM001. As this comparison included the effects of O/M ratio and gap size on pore migration behavior, their effects will be evaluated next.

Comparing with each ceramograph, the 2-D calculation results of temperature and porosity at axial core center at the final power for all B14 test pins are shown in Fig. 25.

For the pins with diametric gap size of 160 μm, i.e. PTM001 and PTM003, the fuel center temperature in PTM003 with O/M ratio of 1.961 was higher than that in PTM001 with O/M ratio of 1.982 due to the effect of O/M ratio on thermal conductivity, as has been described. The calculation results of radial porosity distribution are consistent with results of fuel temperature calculations and are consistent with the O/M influence on central void formation observed in ceramographs. On the other hand, for pins with diametric gap size of 210 μm, i.e. PTM002 and PTM010, the fuel temperature in PTM010 with stoichiometric O/M (1.999) was lower than that in PTM002 with O/M ratio of 1.982, but a larger central void was observed in PTM010 and the central void formation was expected to be accelerated in PTM010. The results of 2-D calculations for these test pins also indicated the same O/M influence on central void formation as PIE results, and this dependence is expected to be caused by the enhanced vapor pressure in the stoichiometric O/M and the accelerated pore migration in PTM010. This effect would be preponderant on pore migration compared to that induced by a higher thermal conductivity reducing temperature in stoichiometric MOX. Okami is capable of accurately representing the accelerated pore migration in stoichiometric MOX due to the highest migration velocity caused by the greatest vapor pressure. The results of comparison between observed and calculated central void diameter in 2-D analysis with Okami are shown in Fig. 26. The porosity at the edge of central void was assumed as 0.5 to define the central void diameter from radial porosity distribution. The central void diameters calculated with Okami were somewhat smaller than the observed ones, but comparably in agreement with PIE results. In this comparison between calculation results and experimental data regarding the central void diameter, we assumed to consider the threshold porosity between fuel matrix and central void as 0.5, which was an empirical value, to determine the central void

diameter. For future works on modeling, this threshold assumed here should be validated by evaluating radial density (or porosity) distribution observed in irradiated MOX fuels.

Based on these results, Okami successfully accounts for the effect of not only gap width but also O/M ratio on central void formation by considering O/M influence on vapor pressure in calculating pore migration velocity.

4.2 Influence of pellet eccentricity

A central void offset from the geometric center of the fuel pellet, as shown in Fig. 27, was observed in ceramograph at the upper position of the fuel column in PTM010 with a larger diametric gap (210 μm). We assumed the pellet eccentricity by using the residual gap to interpret the central void offset, and the fuel temperature and the porosity at this transverse section were calculated in 2-D by using Okami. The 2-D calculation results are shown in Fig. 28. Fuel temperature on the larger-gap side was calculated to be comparably higher than that on the smaller-gap side. According to the radially eccentric profile of fuel temperature, the porosity on the larger-gap side was also higher than that on the smaller-gap side. The radial density profile at this transverse section, calculated with Okami, is shown in Fig. 29. As shown in this figure, the circumferential region with as-fabricated density on the larger-gap side was narrower than that on the smaller-gap side. These results are intuitive based on the relationship between pore migration and large thermal gradients. However, at first glance the calculation results (void offset direction and density profiles) seem to be exactly the opposite of the ceramograph in Fig. 26. This could be explained by the irradiated pellets displacing to the opposite side during sample preparation in PIE from the original location during irradiation.

As a consequence, the 2-D calculations with Okami could represent the central void offset from the geometric center of pellet by taking into account the thermal effects of

various gap sizes circumferentially changing due to the pellet eccentricity on pore migration behavior especially in the large gap cases.

5. Conclusions

In cooperation with INL under the CNWG collaboration between US and Japan, Okami has been developed to evaluate thermal behavior of MOX by installing pore migration models including oxygen potential and vapor pressure to BISON. Pore migration models in Okami account for the effects of fuel composition, i.e. Pu content, MA content, and O/M ratio on pore migration velocity.

Benchmark exercises of fuel temperature and porosity calculations were conducted to compare the calculation results of Okami with CEPTAR, which is verified for fast reactor MOX fuel performance calculations. It was confirmed through a comparison against experimental data, based on the short-term B14 irradiation test, that Okami could calculate the effect of not only O/M ratio but also Am content on pore migration behavior by taking into account their influence on fuel properties such as thermal conductivity and vapor pressure. Also, Okami can adequately simulate the central void offset from the geometric center of a fuel pellet by taking into account the thermal effects of various gap sizes circumferentially changing due to the pellet eccentricity on the corresponding pore migration behavior especially in the large gap cases. As the pore migration behavior regarding fuel restructuring directly affects the fuel temperature evaluation during irradiation, the 2-D analysis which can estimate the effects of pellet eccentricity on the fuel restructuring is very useful to improve the assessment of the safety margin for future advanced fast reactors.

For future development, the pore migration behavior analysis during irradiation

should be validated by comparing the actual radial distribution of fuel density observed in PIE with Okami calculations. The models for redistribution of Pu, MA and oxygen, which is another specific behavior of MOX fuels in fast reactor use, should be applied to fuel performance analysis at the early stage of irradiation. In the next phase, inclusion of a fission gas release model [10], mechanical models for pellet deformation, and burnup dependent properties should be developed to apply fuel performance analyses in long-term irradiation.

References

[1] R. L. Williamson, J. D. Hales, S. R. Novascone, M. R. Tonks, D. R. Gaston, C. J. Permann, D. Andrs, and R. C. Martineau, Multidimensional multiphysics simulation of nuclear fuel behavior, J. Nucl. Mater., 423 (2012) 149-163.

[2] M. Kato, K. Maeda, T. Ozawa, M. Kashimura, Y. Kihara, Physical Properties and Irradiation Behavior Analysis of Np- and Am-Bearing MOX Fuels. J. Nucl. Sci. Technol. 48, No.4, 646-653 (2011).

[3] S. Hirooka, T. Matsumoto, M. Kato, T. Sunaoshi, H. Uno, T. Yamada, Oxygen potential measurement of (U,Pu,Am)O 2 ±x and (U,Pu,Am,Np)O 2 ±x, J. Nucl. Mater. 542 (2020) 152424.

[4] D. R. Olander, Fundamental aspects of nuclear reactor fuel elements, TID-26711-P1, Energy Research and Development Administration, US, 1976, 155–160.

[5] S. Novascone, P. Medvedev, J. W. Peterson, Y. Zhang, and J. Hales, Modeling porosity migration in LWR and fast reactor MOX fuel using the finite element method, J. Nucl. Mater., 508 (2018) 226-236.

[6] T. Ozawa, T. Abe, Development and Verifications of Fast Reactor Fuel Design Code CEPTAR, Nucl. Technol. 156, 39-55 (2006).

[7] T. Ozawa, Analysis of Fast Reactor Fuel Irradiation Behavior in The MA Recycle System, Proc. ICONE25-66129, July 2-6, 2017, Shanghai, China.

[8] D. R. DeHalas, G. R. Horn, Evolution of uranium dioxide structure during irradiation of fuel rods, J. Nucl. Mater. 8 (1963) 207-220.

[9] Y. Ikusawa, K. Maeda, M. Kato, M. Uno, Oxide-Metal Ratio Dependence of Central Void Formation of Mixed Oxide Fuel Irradiated in Fast Reactors, Nucl. Technol. 199, 83-95 (2017).

[10] F. Verdolin, S. Novascone, D. Pizzocri, G. Pastore, T. Barani, L. Luzzi, Modelling fission gas behavior in fast reactor (U,Pu)O2 fuel with BISON, J. Nucl. Mater., 547 (2021) 152728.

List of figures and tables

Fig. 29 Radial density profile calculated for transverse section at the same position of cerampograph at the upper position of fuel column in PTM010.

Table 1 Conditions of benchmark exercises for pore migration model.

1-D calculations	Exercise 1	Exercise 2
System	4.1 mm radius x 100 mm height	2.675 mm radius x 100 mm height
Initial conditions	- Porosity 0.12 - Temperature 1,400 K	- Porosity 0.15 - Temperature 630 K
Boundary conditions	- Outer surface temperature 1,400 K - Pore migration flux at boundary (outer surface) is zero.	- Outer surface temperature 1,000 K - Pore migration flux at boundary (outer surface) is zero.

Table 2 Major specifications of four test pins irradiated in B14.

Pin ID	PTM001	PTM002	PTM003	PTM010
Cladding material	PNC316			
Cladding outer diameter	6.50 mm			
Cladding inner diameter	5.56 mm			
Fuel type	Am-MOX			
Pellet type	Solid			
Fuel column length	400 mm			
Pu content	31 wt.%HM			
Am content	2.4 wt.%HM			
O/M ratio (as-fab.)	1.982	1.982	1.961	1.999
Fuel pellet diameter (Pellet-cladding gap size)	5.40 mm (160 μm)	5.35 mm (210 μm)	5.40 mm (160 μm)	5.35 mm (210 μm)
Fuel density (as-fab.)	85.7 %T.D.	85.7 %T.D.	85.4 %T.D.	85.2 %T.D.

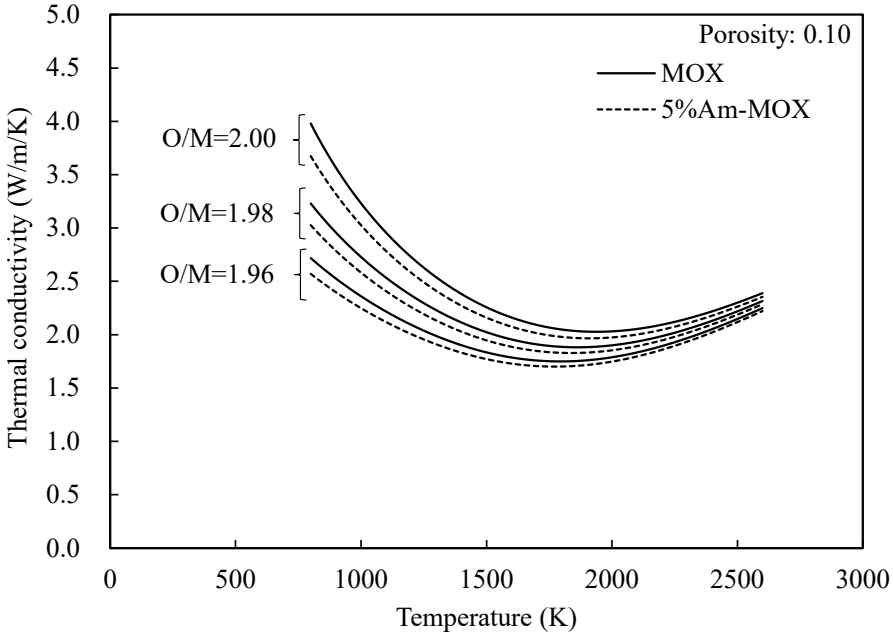

Fig. 1 O/M dependence of fuel thermal conductivity.

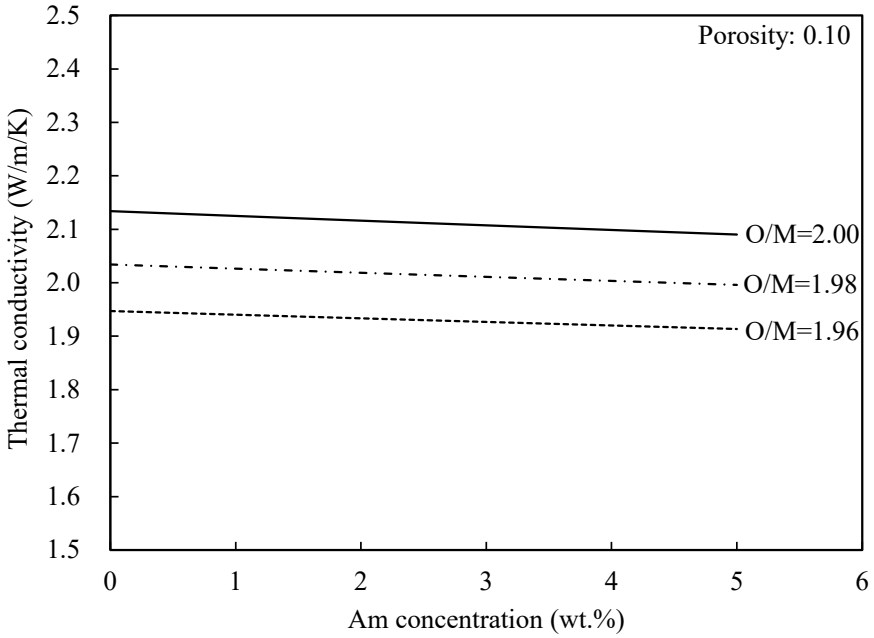

Fig. 2 Am content dependence of fuel thermal conductivity at 2,273 K.

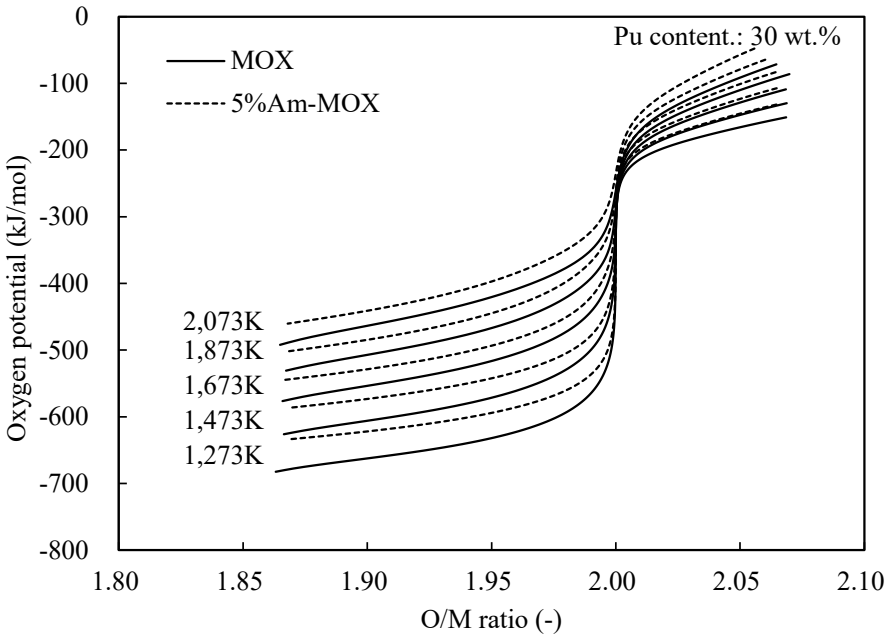

Fig. 3 O/M dependence of oxygen potential.

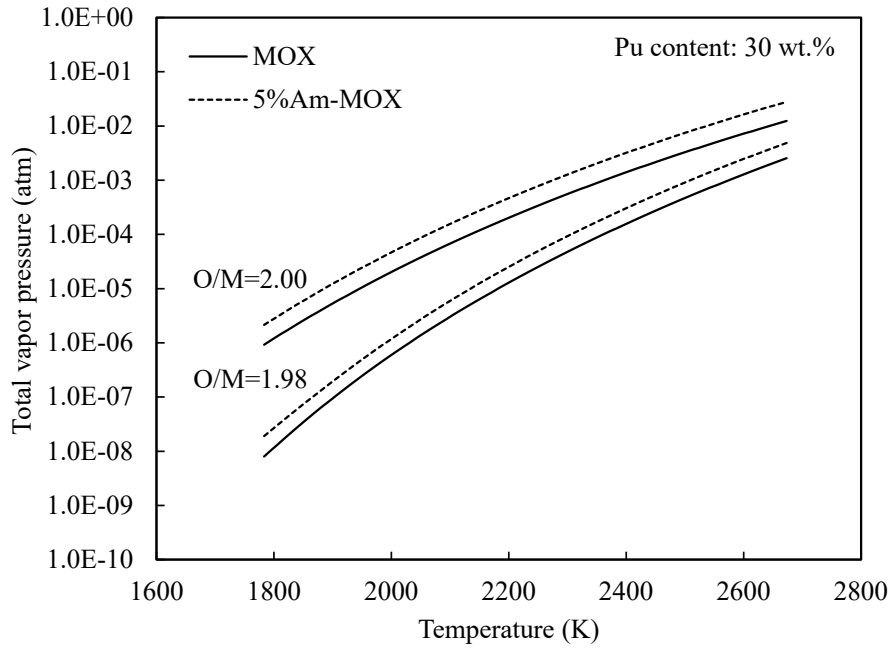

Fig. 4 O/M dependence of total vapor pressure.

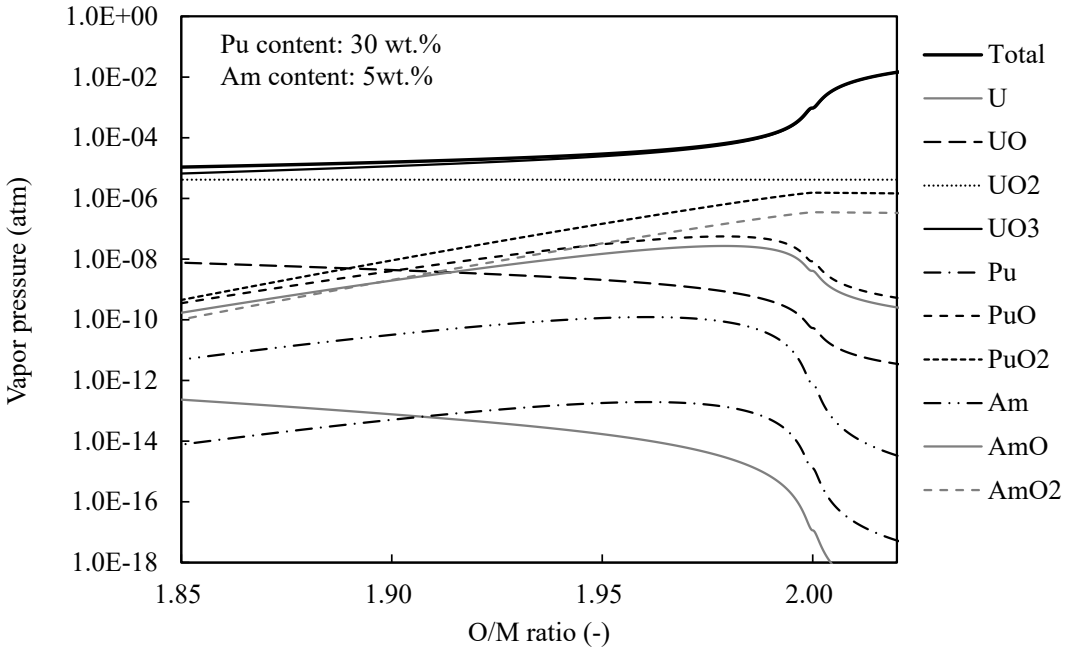

Fig. 5 O/M dependence of vapor pressure of each vapor specie and total vapor pressure of 5 wt.%Am-bearing MOX at 2,273 K.

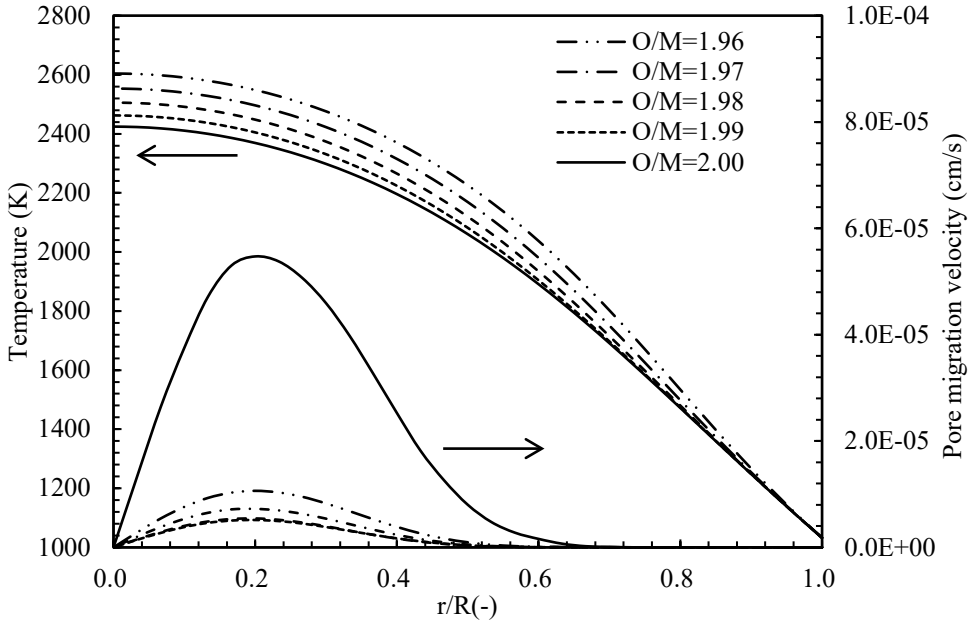

Fig. 6 Effect of O/M ratio on fuel temperature and pore migration velocity (Am content: 5 wt.%).

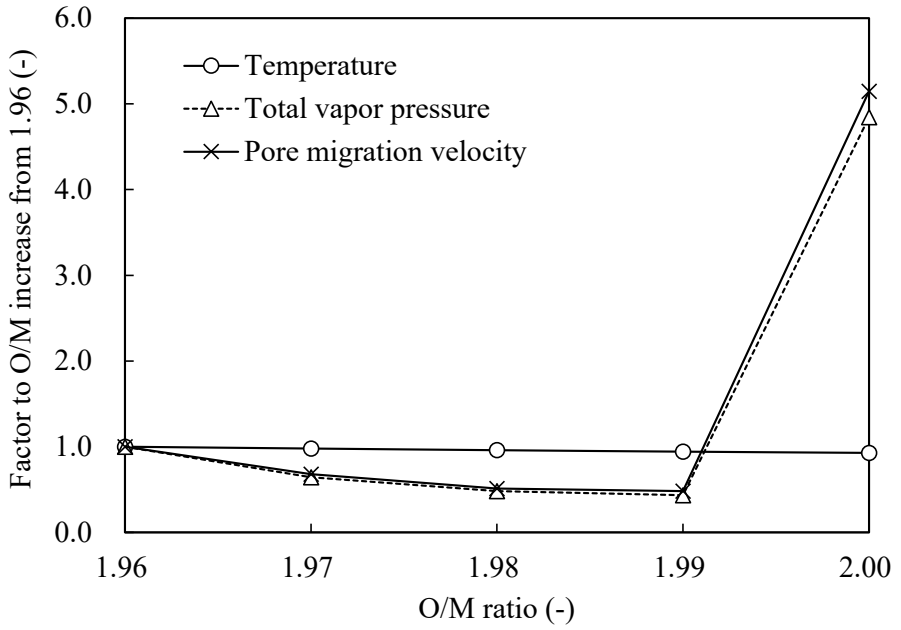

Fig. 7 Factor of temperature, total vapor pressure and pore migration velocity to O/M increase from 1.96 at r/R = 0.2 (Am content: 5 wt.%).

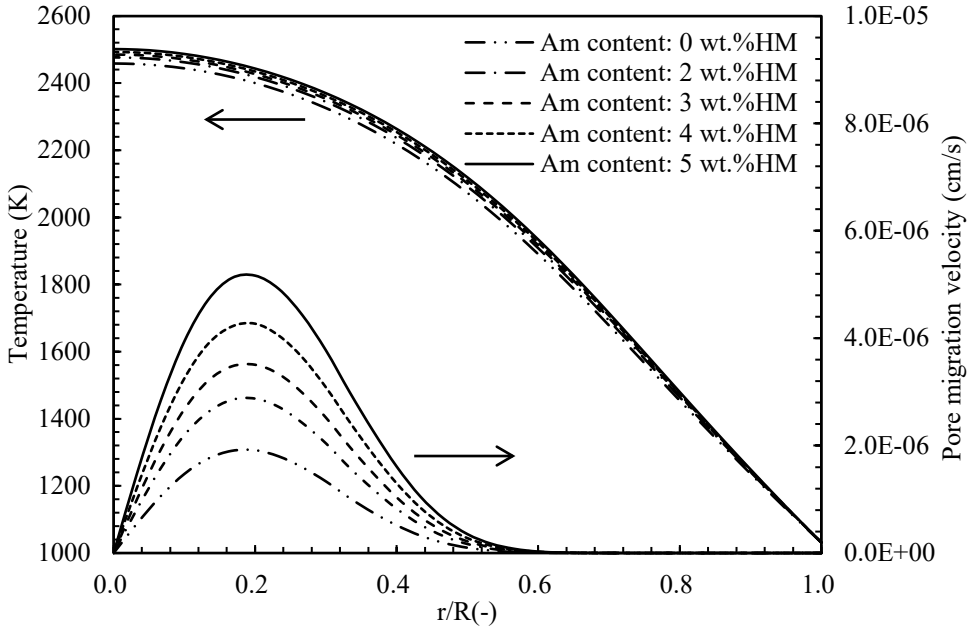

Fig. 8 Effect of Am content on fuel temperature and pore migration velocity (O/M: 1.98).

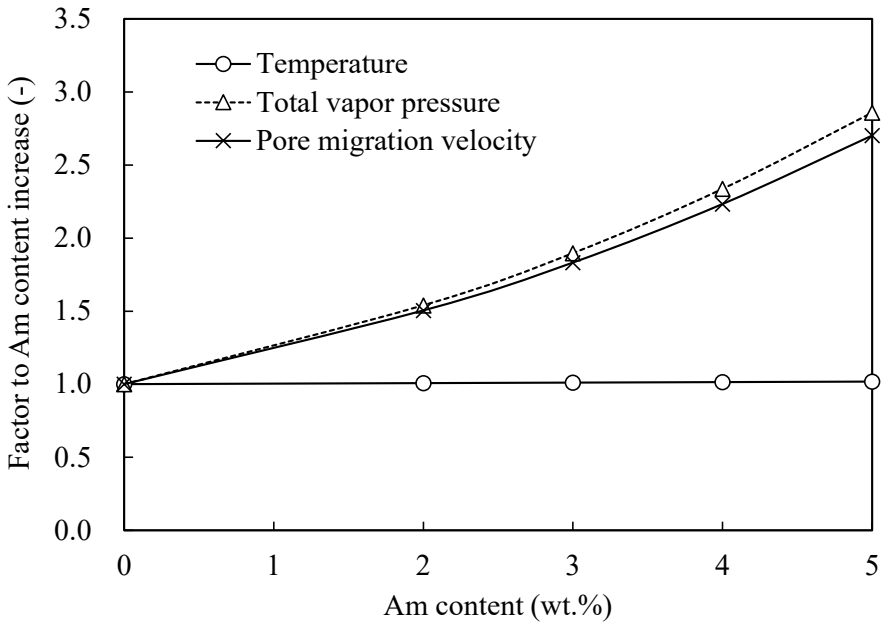

Fig. 9 Factor of temperature, total vapor pressure and pore migration velocity to Am content increase at r/R = 0.2 (O/M: 1.98).

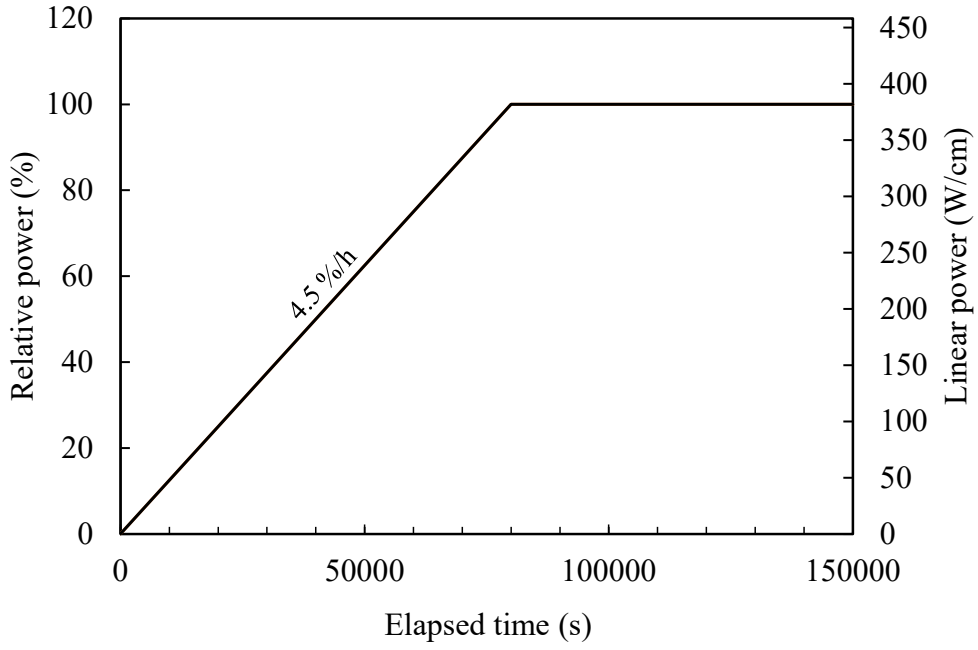

Fig. 10 Power history assumed for exercise 1.

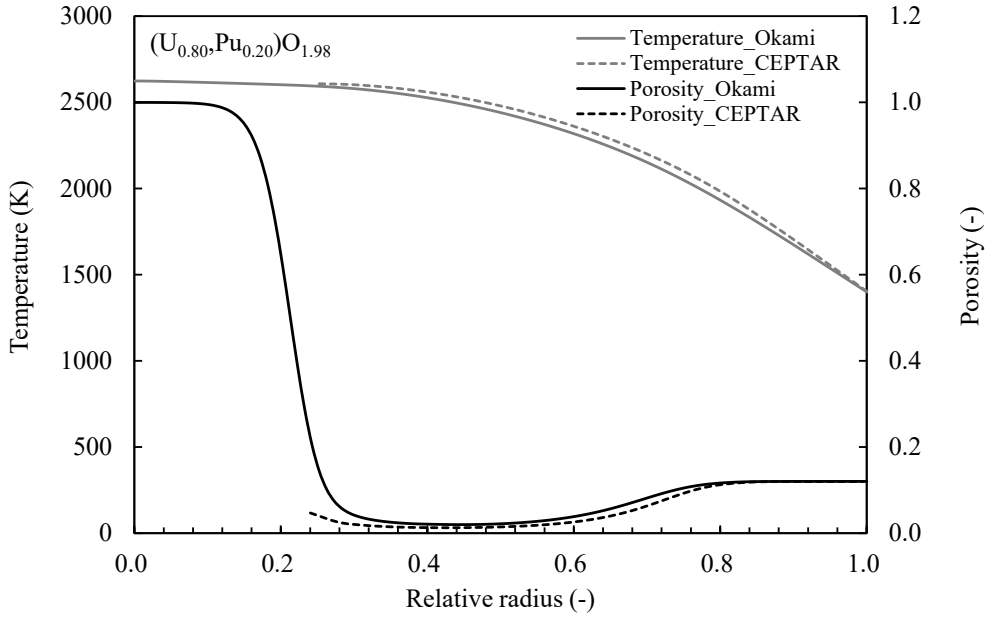

Fig. 11 Comparison of temperature and porosity between CEPTAR and Okami at elapsed time of 150,000 s (O/M=1.98).

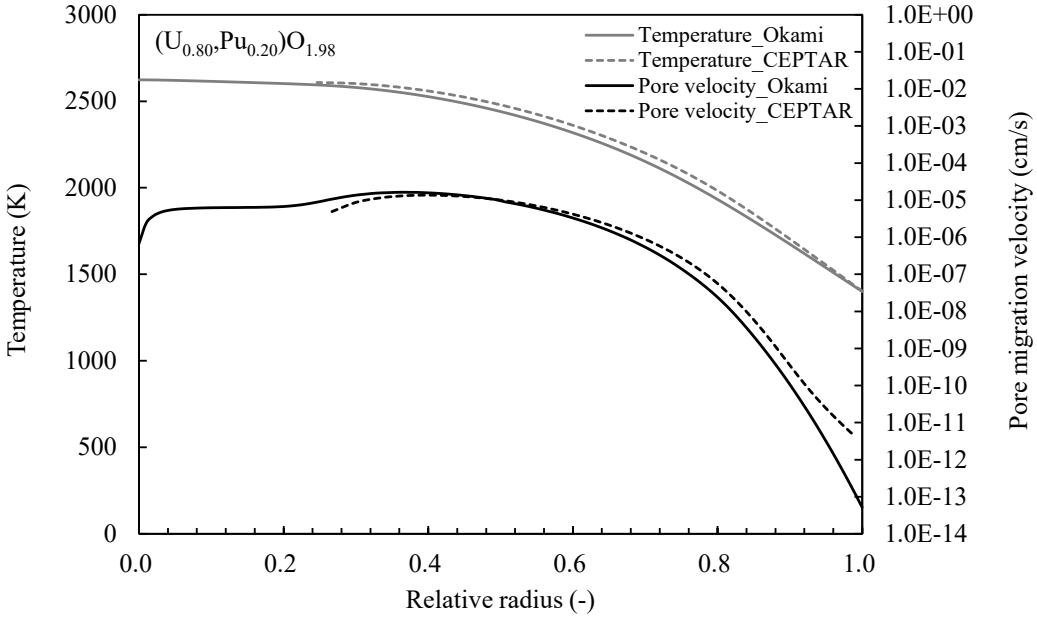

Fig 12 Comparison of temperature and pore migration velocity between CEPTAR and Okami at elapsed time of 150,000 s (O/M=1.98).

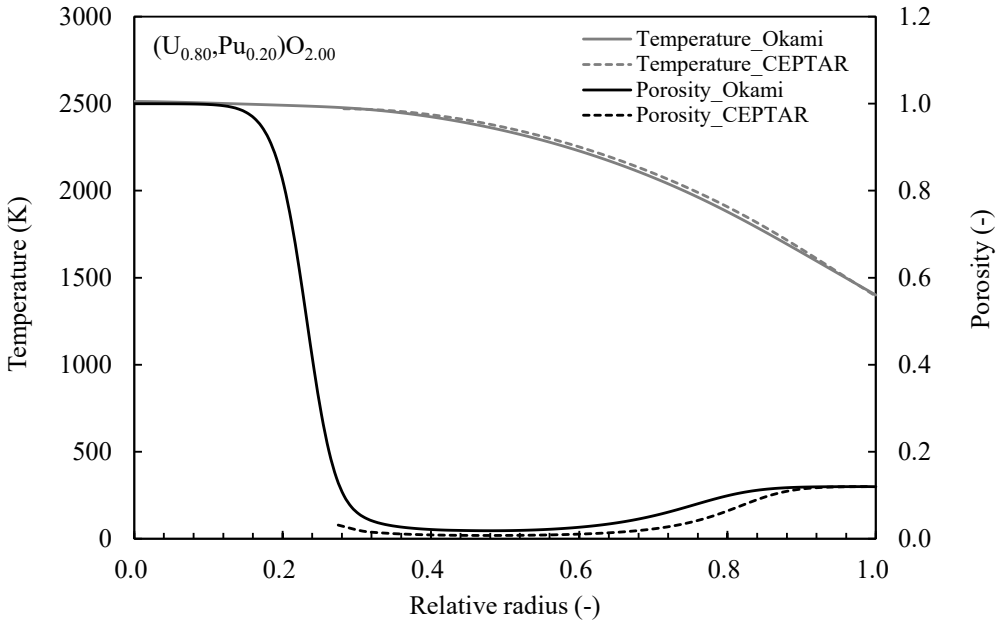

Fig. 13 Comparison of temperature and porosity between CEPTAR and Okami at elapsed time of 150,000 s (O/M=2.00).

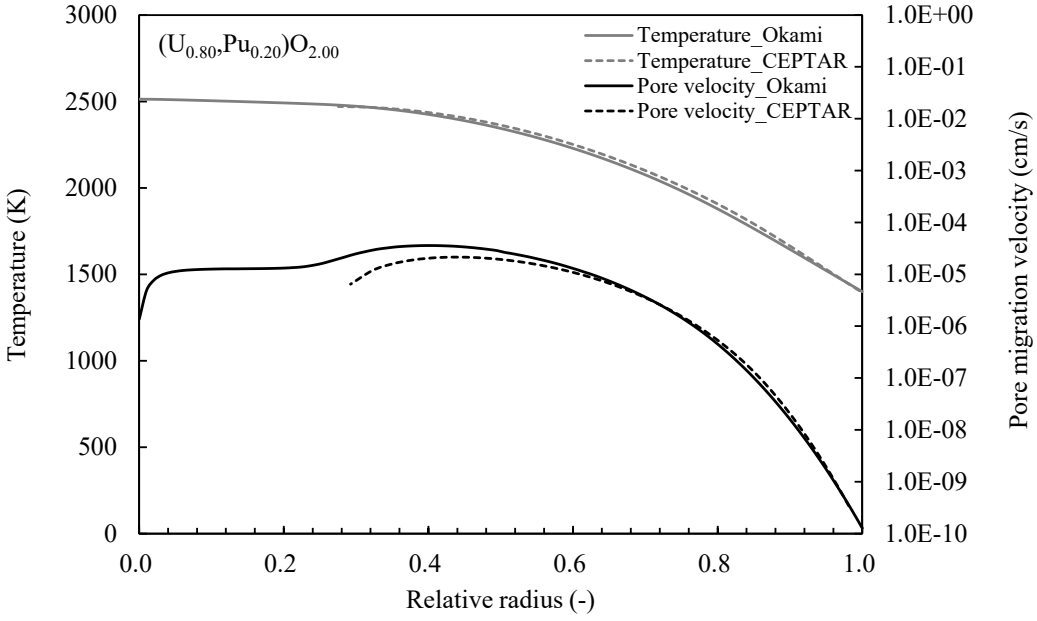

Fig. 14 Comparison of temperature and pore migration velocity between CEPTAR and Okami at elapsed time of 150,000 s (O/M=2.00).

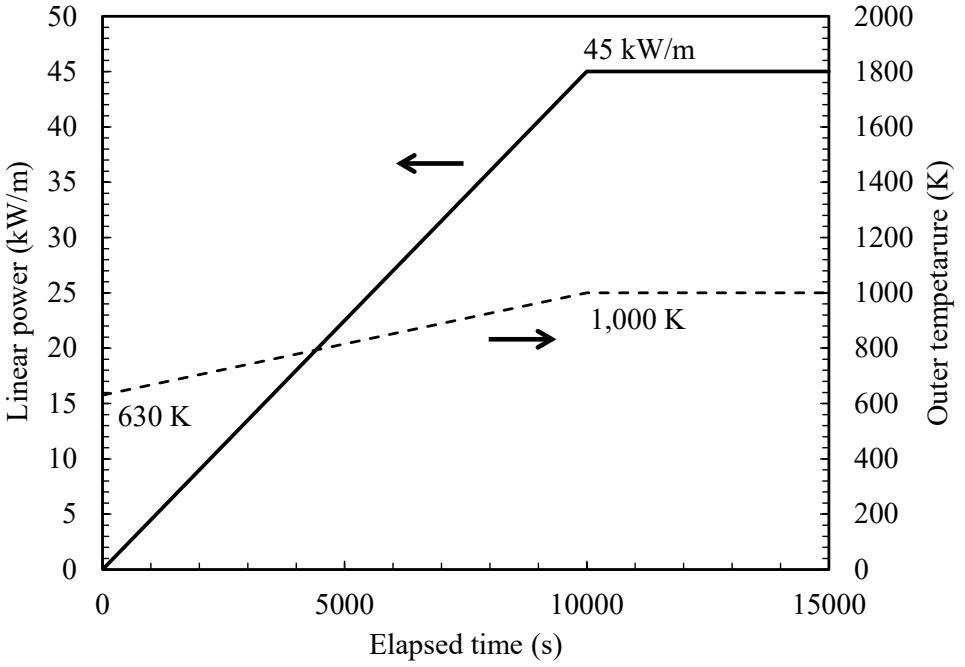

Fig. 15 Power history and outer surface temperature assumed for exercise 2.

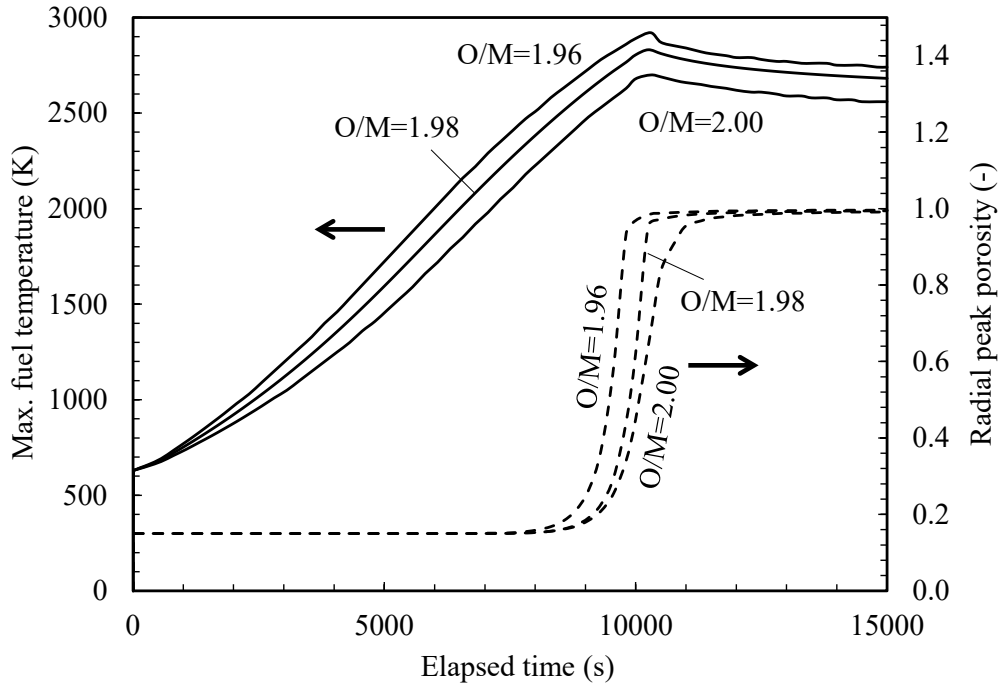

Fig. 16 Comparison of max. fuel temperature and max. porosity among O/M ratio of 1.96, 1.98 and 2.00.

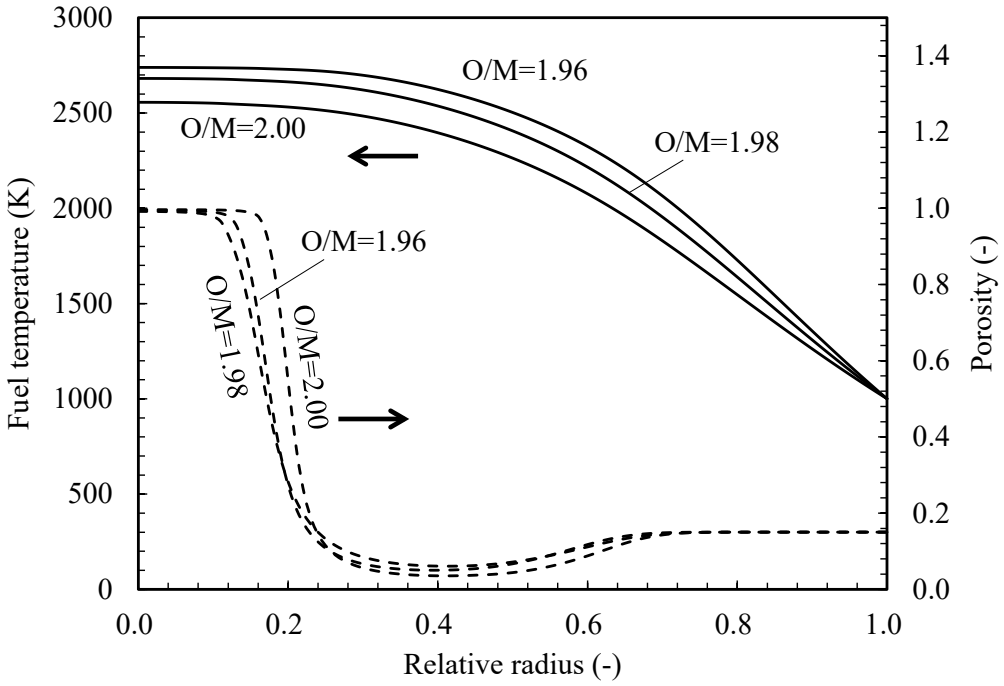

Fig. 17 Comparison of radial profile of fuel temperature and porosity among O/M ratio of 1.96, 1.98 and 2.00.

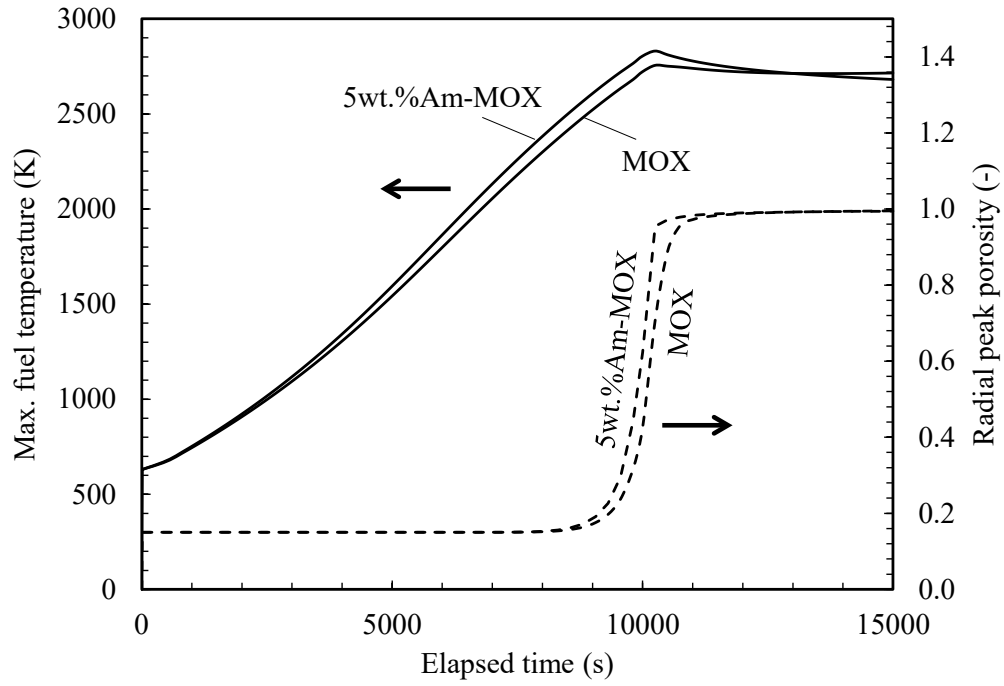

Fig. 18 Comparison of max. fuel temperature and max. porosity between MOX and 5wt.%Am-MOX.

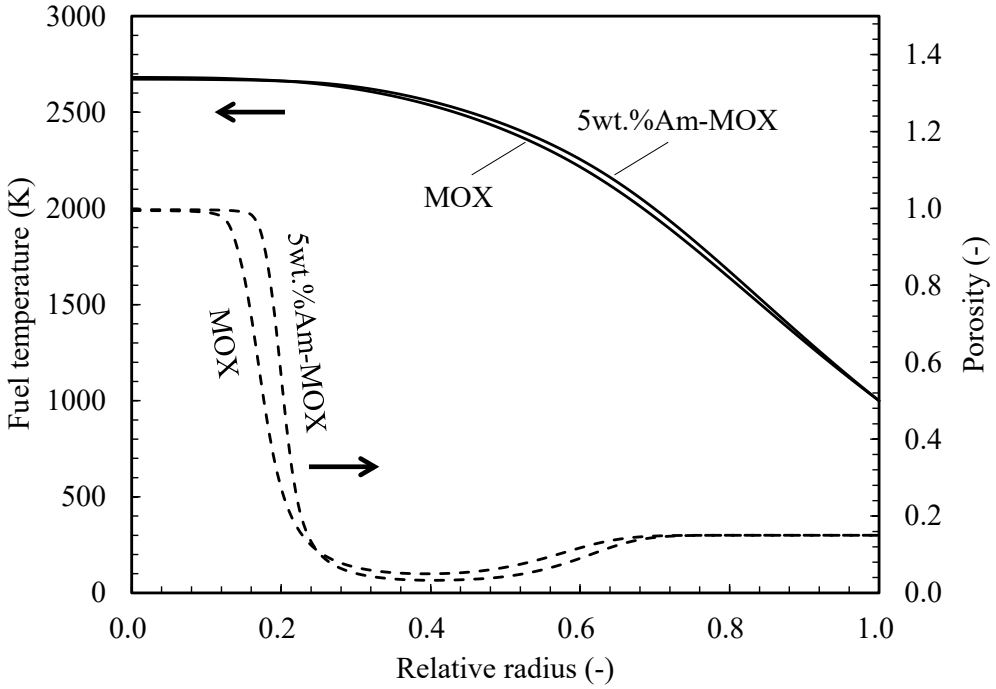

Fig. 19 Comparison of radial profile of fuel temperature and porosity between MOX and 5wt.%Am-MOX.

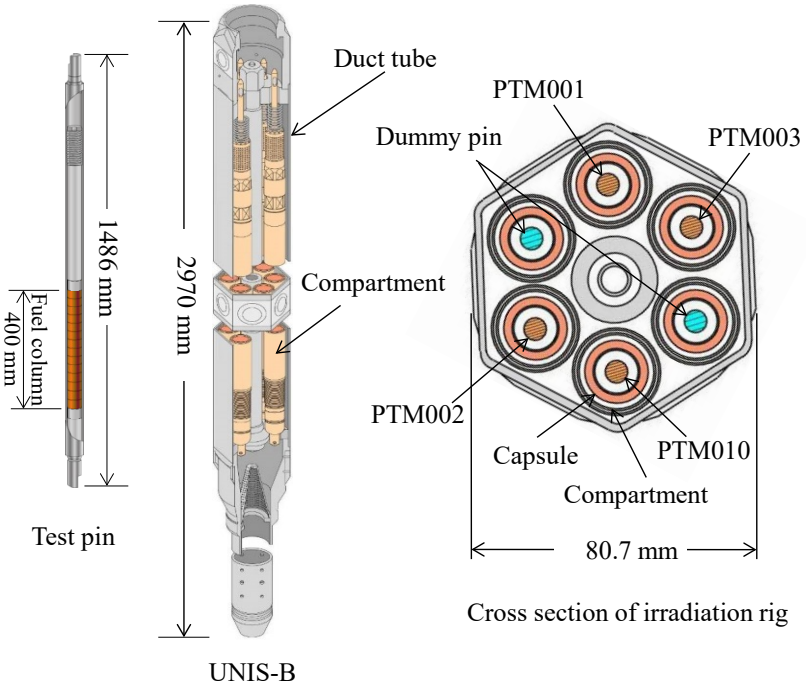

Fig. 20 Schema of UNIS-B and test pins used for B14 test.

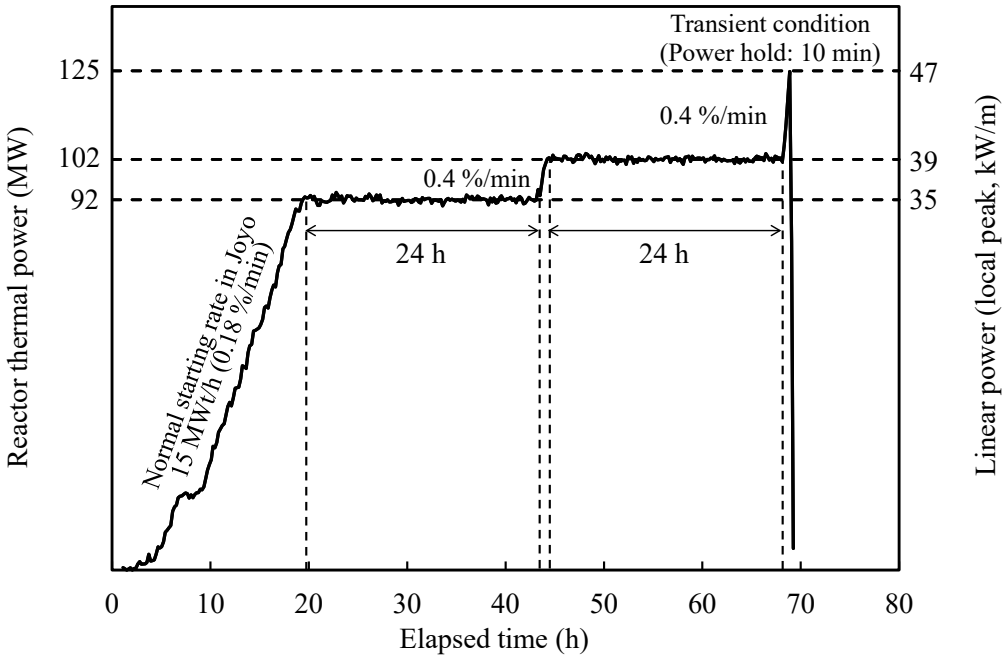

Fig. 21 History of reactor power and local peak linear power during B14 test.

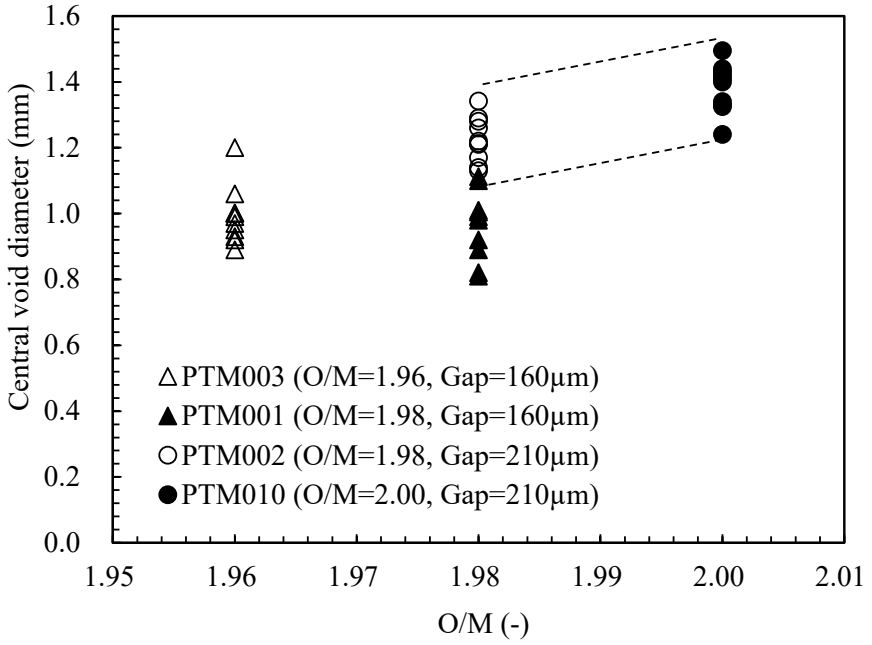

Fig. 22 Influence of O/M ratio on central void diameter observed in B14 test pins.

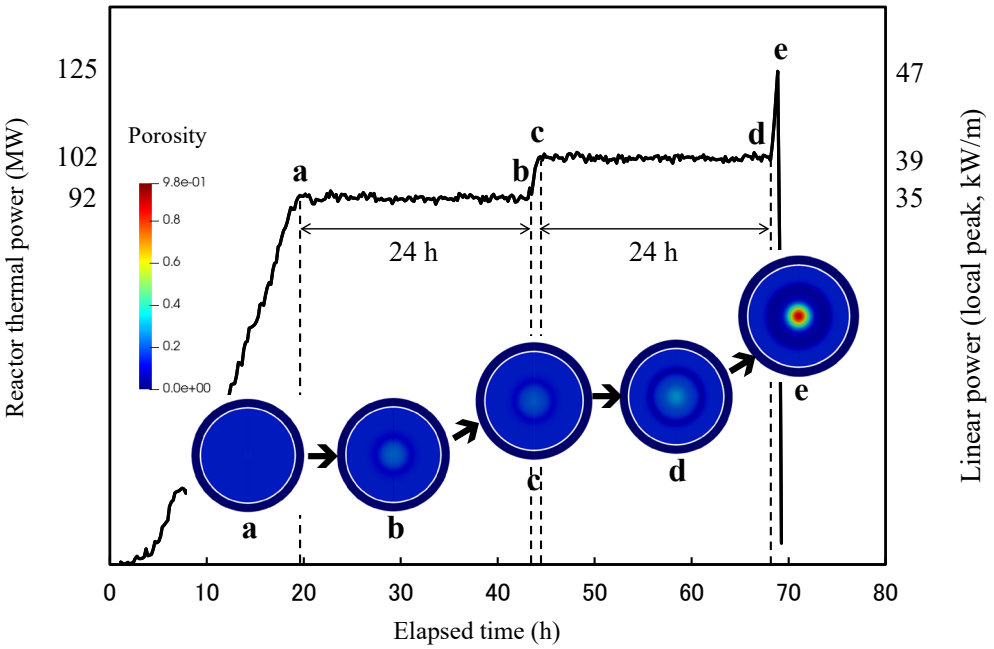

Fig. 23 Pore migration process for PTM001 during B14 test.

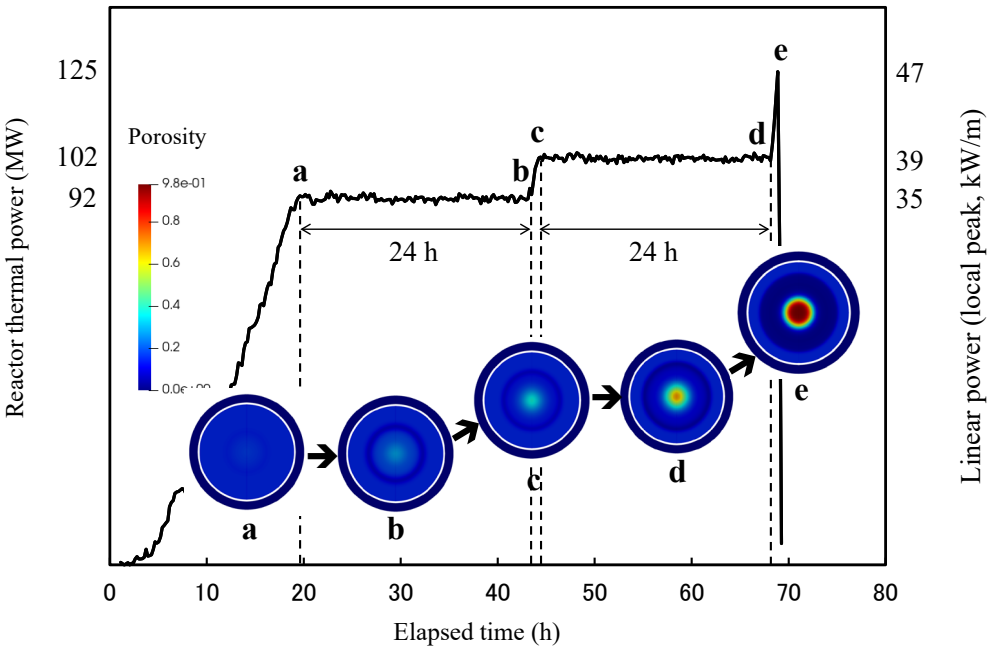

Fig. 24 Pore migration process for PTM010 during B14 test.

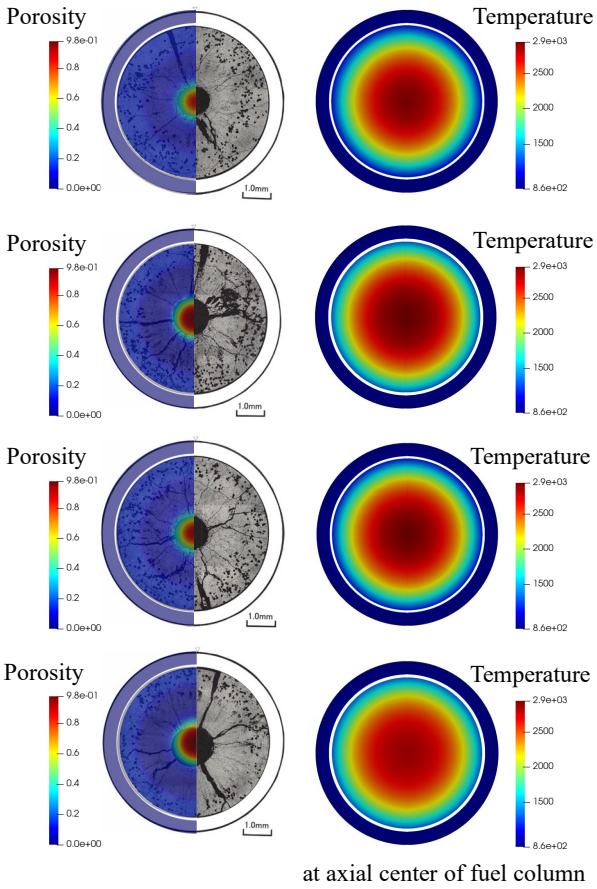

PTM001
DFCC: +33 mm
O/M: 1.982
Diametric gap size: 160 μm
Max. LHR: 47.2 kW/m
Cladding outer temp.: 593 ºC

PTM002
DFCC: +27 mm
O/M: 1.982
Diametric gap size: 210 μm
Max. LHR: 46.1 kW/m
Cladding outer temp.: 584 ºC

PTM003
DFCC: +33 mm
O/M: 1.961
Diametric gap size: 160 μm
Max. LHR: 46.1 kW/m
Cladding outer temp.: 588 ºC

PTM010
DFCC: +25 mm
O/M: 1.999
Diametric gap size: 210 μm
Max. LHR: 46.3 kW/m
Cladding outer temp.: 588 ºC

Fig. 25 2-D calculation results of porosity and temperature at axial center of fuel column at the final power in B14 test pins.

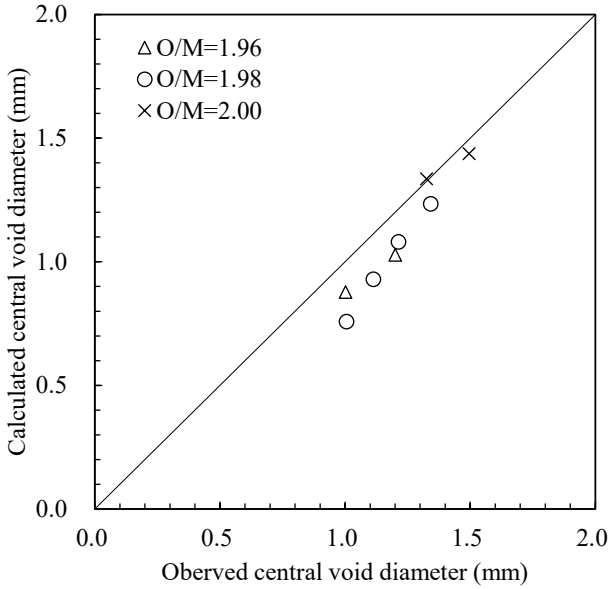

Fig. 26 Comparison between the central void diameters observed in PIE and those calculated in 2-D analysis with Okami.

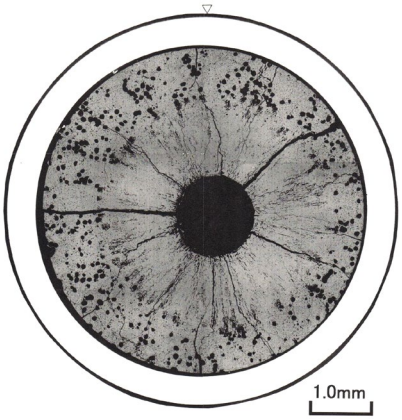

PTM010
DFCC: +97 mm
O/M: 1.999
Diametric gap size: 210 μm
Max. LHR: 43.9 kW/m
Cladding outer temp.: 610 ºC

Fig. 27 Ceramograph at the upper position of fuel column in PTM010.

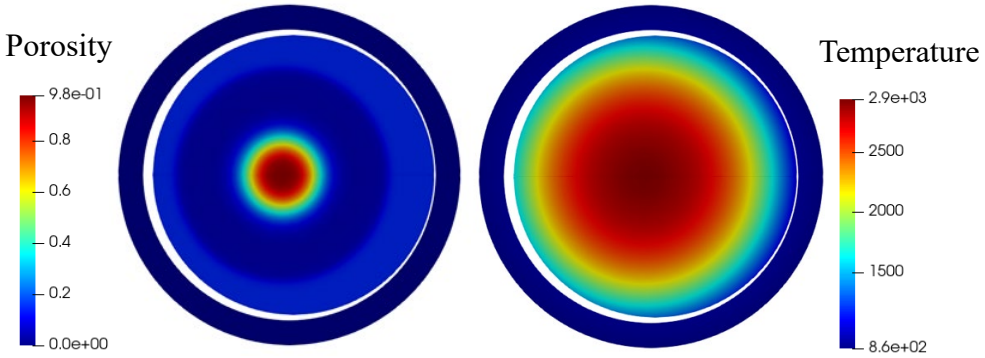

Fig. 28 2-D calculation results of transverse section at the same position of cerampograph at the upper position of fuel column in PTM010.

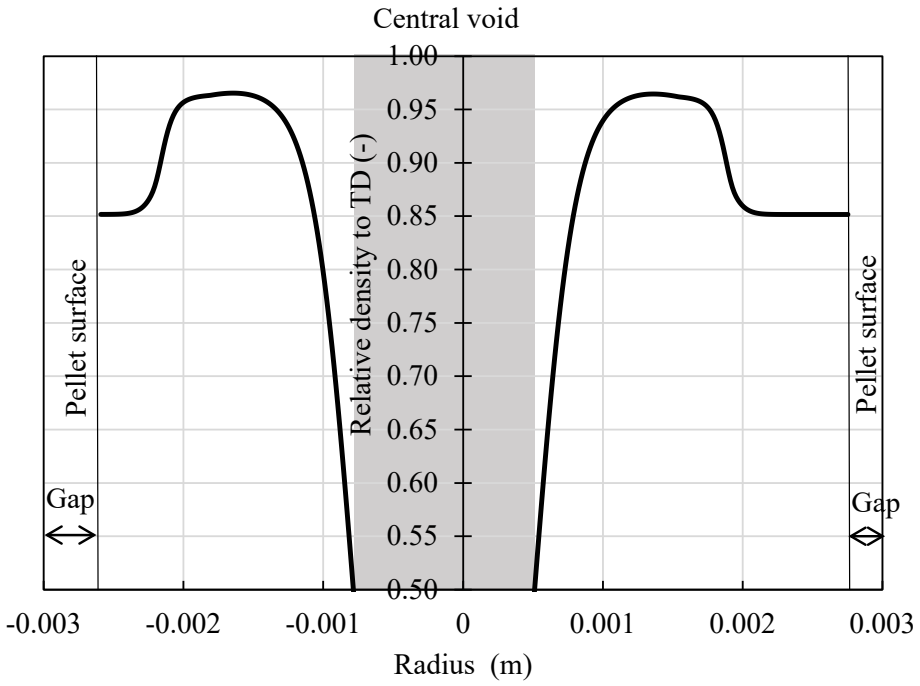

Fig. 29 Radial density profile calculated for transverse section at the same position of cerampograph at the upper position of fuel column in PTM010.